ARTICLE NO. 78-1216R

J80-120

Pressure Wave Suppression for a Pulsed Chemical Laser

20001
20009
30012

William J. Thayer III,* Victor R. Buonadonna,† and William D. Sherman‡
Boeing Aerospace Co., Seattle, Wash.

Analyses and experiments were carried out to characterize mechanisms and techniques which control medium uniformity during repetitively pulsed DF/HF laser operation. Density uniformity was shown analytically to be controlled by residual, nonacoustic density variation ("entropy waves"). The dependence of these disturbances on measured pressure fluctuations was determined interferometrically. Analysis led to development of a pressure wave attenuator utilizing water sprays and viscous damping material. Using this device, suppression of pressure disturbances to $\Delta p/p \cong 4\times 10^{-3}$ was demonstrated within 6 ms after reaction at a 50-Hz pulse rate for several $F_2/H_2/He$ mixtures, and within 3.6 ms at 84 Hz. Entropy wave density nonuniformities of $(\Delta\rho/\rho)_{rms} \leq 10^{-3}$ were achieved in times consistent with mass utilization efficiency of 50% or higher.

I. Introduction

OPERATION of a repetitively pulsed chemical laser involves a number of periodic flow processes. Reagents and diluent, such as D_2, F_2, and He for a DF laser, are mixed on the fly and convected into the laser cavity, such as shown in Fig. 1, prior to each laser pulse. When the cavity is filled with a uniform mixture, an external means such as an ultra violet or electron beam pulse is used to initiate chemical reaction which proceeds to completion in 10-20 μs. Since only a small fraction of the chemical energy released by the D_2-F_2 reaction is extracted as light, most of this energy is rapidly thermalized within the laser cavity in an essentially constant-volume heat release pulse. The resulting local equilibrium temperature and pressure, up to 3500 K and 12 atm, respectively, from ambient initial conditions, produce large-amplitude unsteady gas flow throughout the laser flow channel. Chemical reaction must then be extinguished and both reaction products and pressure disturbances must be cleared from the laser cavity so that the cavity can be refilled with fresh, uniform reagent mixture. This sequence is then repeated. Operation at high average power requires that lasing take place at pulse rates of 20-100 Hz or higher.

Several critical fluid dynamics problems are associated with supplying D_2-F_2-diluent mixtures having very high concentration, temperature, and density uniformity to a pulsed laser cavity. These problems include extinguishing the chemical reaction following each laser pulse, uniform distribution of reagents throughout the three dimensions of the laser cavity, homogeneous mixing of the reagent streams, and suppression of pressure and density disturbances prior to refilling the cavity for each laser pulse. Development of a high power pulsed chemical laser requires that all of these problems be recognized and successfully dealt with in the flow apparatus. In addition, efficient device operation imposes the constraint that at least half of the total gas flow be used for lasing. This constraint places severe requirements on the reagent supply system response, mixer length and volume, and on the time available for pressure disturbance suppression. Modeling and development of a reagent supply, injector, and mixer that provide regions of uniform concentration reagent mixture to the laser cavity, separated by nonreactive regions to extinguish reaction, are described in detail in Ref. 1. Development and demonstration of techniques for suppressing pressure disturbances following each reaction pulse are the subjects of this paper.

The refractive index of the lasing medium must be spatially uniform to support a near diffraction limited beam quality. Since refractive index is related directly to the gas density, this requirement for good beam quality places a density uniformity requirement $\Delta\rho/\rho$ on flow quality. The required $\Delta\rho/\rho$ can be estimated by using the expression for the central peak far-field intensity I normalized with respect to its diffraction limited value I_0,

$$I/I_0 = e^{-(\Delta\phi)^2}$$

where

$$\Delta\phi \simeq (2\pi L/\lambda)\beta\rho(\Delta\rho/\rho)_{rms}$$

and L is the optical path length ($\sim$200 cm for large device), λ the wavelength (3.8×10^{-4} cm), β the Gladstone Dale constant ($\sim 0.9\times 10^{-4}$), and ρ the density ($\sim$1 amagat). The generally acceptable value for I/I_0 is 0.83 (1.2 $\times$ diffraction limited beam), resulting in $(\Delta\rho/\rho)_{rms} \sim 10^{-3}$. Thus the maximum allowable density nonuniformity in the laser cavity must be less than 10^{-3} at the time of each laser pulse for near diffraction limited beam quality.

Strong shock and expansion waves are generated within the flow cavity by the reaction pulse. These strong waves are cleared from the cavity in a relatively short time, generally 2-3 ms. (During this short time internal the hydrogen flow is turned off in order to obtain flame out.) For properly designed attenuators, only small residual pressure disturbances will continue to reverberate throughout the flow cavity after this period. These reverberating waves are the disturbances of primary interest in this study since they affect the density uniformity of the fresh H_2-F_2 gas mixture flowing into the cavity. These pressure waves produce density nonuniformities through two principal mechanisms: direct isentropic compression or expansion of the gas within the laser cavity, and nonisentropic state changes produced by interaction of the pressure disturbances with sonic injector jets. The isentropic disturbances propagate through the cavity region at the acoustic speed; whereas the nonisentropic disturbances, often called "entropy waves," are convected downstream at the mean flow velocity. An analysis that showed that density nonuniformity at the time of each laser pulse is controlled by these entropy waves is described in Sec. II. The analysis also identified mechanisms which controled the suppression of pressure disturbances and was used to

Presented as Paper 78-1216 at the AIAA 11th Fluid and Plasma Dynamics Conference, Seattle, Wash., July 10-12, 1978; submitted Aug. 30, 1978; revision received Oct. 15, 1979.

Index categories: Lasers; Aeroacoustics; Nonsteady Aerodynamics.

*Presently, Principal Reseach Scientist, Mathematical Sciences, N.W., Bellevue, Wash. Member AIAA.

†Senior Specialist Engineer, Laser Physics Group. Member AIAA.

‡Senior Engineer, Laser Physics Group. Member AIAA.

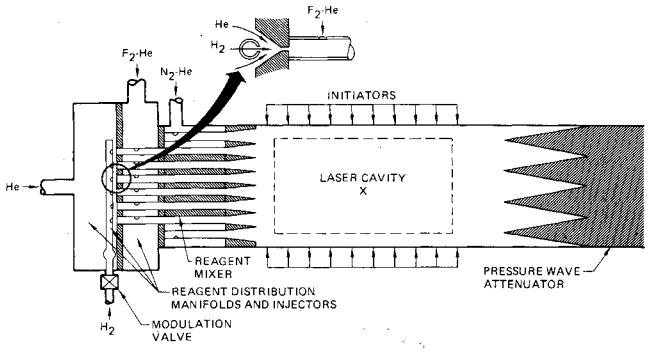

Fig. 1 Schematic of repetitively pulsed DF(HF) laser flow system.

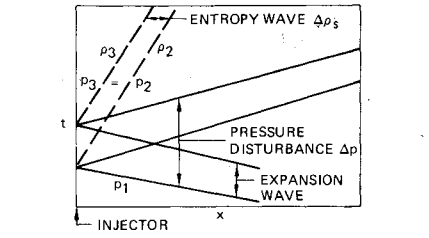

a) WAVE DIAGRAM DURING ENTROPY WAVE FORMATION

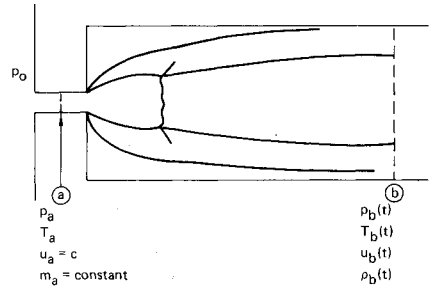

b) CONTROL VOLUME OF QUASISTEADY FLOW MODEL

Fig. 2 Quasisteady flow model of entropy wave formation.

develop the attenuation technique described in Sec. III. Suppression of pressure disturbances to an acceptable level was demonstrated experimentally using this attenuator, as discussed in Sec. IV.

II. Analysis

Relations Between Density and Pressure Disturbances

Density variations which are produced by residual pressure disturbances are considered here. These density variations are due to both isentropic and nonisentropic processes. The analysis to follow shows that the nonisentropic disturbances (entropy waves) dominate pressure wave suppression requirements for the wavelengths and wave amplitudes expected in a pulsed laser and observed in flow experiments.

Sonic orifices are used within the injector to isolate the reagent supply from the reaction produced overpressures. Nonisentropic variations in the final state of gas entering the flow channel through these choked injector orifices are produced by changes in jet pressure recovery caused by pressure disturbances in the mixer and cavity. Since these entropy waves (density disturbances) travel through the cavity at the mean stream velocity, they require a much longer time (more than an order of magnitude longer for high mass utilization efficiency, 50-Hz operation) to clear the cavity than the pressure disturbances. A simple analysis of the pressure recovery process downstream of the injector orifices was carried out to determine the magnitude of density disturbances associated with entropy waves and their dependence on pressure wave amplitude.

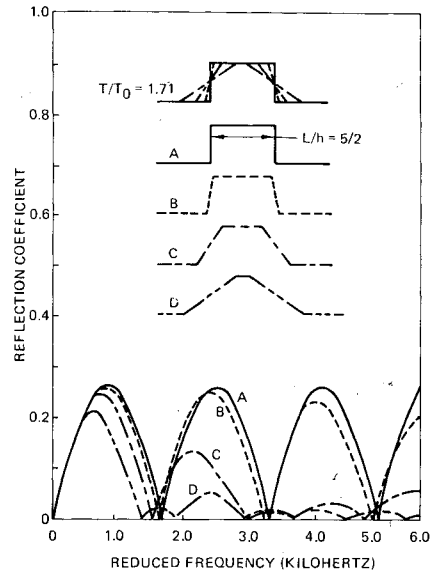

Fig. 3 Effect of axial temperature gradient on reflection coefficient in uniform duct.

A quasisteady flow model was used to characterize the entropy wave phenomenon. Mass flow rate through the injector is constant throughout the laser cycle since flow through the orifices is choked. The x-t diagram of Fig. 2a shows the reflection of a pressure wave from the injector, producing a pressure change from p_1 to $p_2 = p_1 - \Delta p$, and an isentropic density change from ρ_1 to ρ_2. Before the arrival of the unsteady flow disturbance, flow is steady in the cavity at pressure p_1. After the pressure disturbance has left this region, the cavity pressure is constant at p_2. Gas which is injected after the pressure wave reflection has a different density, ρ_3, than that injected before or during the pressure wave interaction. It is the net change in density, $\Delta\rho_s = \rho_2 - \rho_3$, of the entropy wave produced by the net pressure change, $\Delta p = p_1 - p_2$, that is of interest.

The ideal gas equation of state and steady flow mass and energy conservation equations applied to the control volume of Fig. 2b can be solved simultaneously to evaluate the downstream conditions ρ_b, u_b, T_b for a prescribed pressure p_b and the known injector orifice conditions, p_a, ρ_a, u_a, T_a. The density of gas at state 2 is evaluated from that at state 1 by using the isentropic ideal gas relation across the unsteady flow expansion Δp. These equations can be combined to give the following relationship between the entropy wave density nonuniformity $\Delta\rho_s$ an the overall pressure change Δp;

$$\frac{\Delta\rho_s}{\rho} = -1 + \left(1 + \frac{\Delta p}{p}\right)^{\frac{\gamma-1}{\gamma}} \left\{ \frac{1 + \frac{\gamma-1}{2} M_a^2 \left[1 - \left(\frac{u_3}{u_a}\right)^2\right]}{1 + \frac{\gamma-1}{2} M_a^2 \left[1 - \left(\frac{u_1}{u_a}\right)^2\right]} \right\} \tag{1}$$

where M_a is the Mach number at the inlet orifice and separate expressions are available for u_3/u_a and u_1/u_a. Since u_a is the sound speed for injectors of interest, and u_1 and u_3 are low velocities, $(u_1/u_a)^2$, $(u_3/u_a)^2 \ll 1$. For small pressure disturbances and low cavity Mach number, this equation reduces to

$$\frac{\Delta\rho_s}{\rho} = \frac{\gamma-1}{\gamma}\frac{\Delta p}{p} = K\frac{\Delta p}{p} \tag{2}$$

For mixtures of interest for pulsed laser applications, the constant K is approximately 0.38. This expression overestimates the entropy wave magnitude due to, e.g., finite amplitude pressure disturbances, moderate flow velocity, and

axial entropy disturbance spreading in the mixer (see Sec. IV). However, it is useful for estimating the required pressure wave suppression at the time the cavity fill begins. The "wavelength" of the entropy wave (λ_s) is considerably shorter than the pressure disturbance wavelength (λ_p), as can be readily ascertained from the x-t diagram of Fig. 2a. It is easily shown that for weak acoustic pressure waves, $\lambda_s/\lambda_p = M/(1-M)$, where M is the convective flow Mach number. Because of this wavelength compression effect, entropy waves are expected to be on the order of 10-30 cm in length and persist across the cavity along the optic axis. The required density uniformity for large scale disturbances of this form is $\Delta\rho/\rho \simeq 10^{-3}$. Equation (2) then implies that pressure disturbances must be suppressed to $\Delta p/p \simeq 2.6 \times 10^{-3}$ prior to the start of cavity fill. Timing requirements for mass utilization efficiency above 50% show that pressure wave attenuation to this level must be accomplished within 4-6 ms after the reaction pulse for 50 Hz operation.[1]

The isentropic density variation $\Delta\rho_a$ due to pressure disturbances present in the laser cavity at the time of each laser pulse must be considered in addition to the entropy disturbances. Note that pressure disturbances present at the pulse must be quite small, i.e., $\Delta p/p < 3 \times 10^{-3}$, for entropy related density nonuniformity to be acceptable. For small pressure disturbances,

$$\frac{\Delta\rho_a}{\rho} = \frac{1}{\gamma}\frac{\Delta p}{p} \tag{3}$$

This indicates that isentropic density disturbances may have amplitudes comparable to the entropy disturbances. However, the unsteady flow calculations and experimental data discussed below show that pressure disturbances that remain in a properly designed device at the time of a laser pulse have very long wavelengths, on the order of 200 cm or more, and are repeatable from pulse to pulse. These wavelengths are much larger than typical laser cavity lengths of 20-40 cm in the flow direction. It may be shown[1] that for pressure disturbances with wavelengths much longer than the cavity length, isentropic density disturbances present in the cavity at any time are only 1-10% of the peak to peak disturbance. Hence, isentropic density variation at the time of a laser pulse is much less than the entropy variation associated with pressure waves of the same amplitude and wavelength.

Modeling of Pressure Wave Suppression

Several existing computer programs were applied to evaluate pressure wave suppression devices and to identify controlling mechanisms. An acoustic transmission code[2] was used to study the effects of duct geometry, damping material configuration, duct termination, and internal gas temperature gradients in the limit of small pressure disturbances. Inviscid, unsteady flow calculations were made to evaluate effects of duct geometry on strong pressure disturbance clearing from the cavity.[3] Additional unsteady flow calculations were carried out using the Poseidon Research computer program[4] to evaluate effects of viscous damping and heat extraction from reaction products. Some results of these calculations are discussed below, and more detailed information is available in Ref. 1. Time and resource constraints during the subject program did not allow development of a computer code that modeled pressure wave suppression by a combination of water sprays and stationary damping material as used in the test program.

A principal result of the acoustic transmission calculations was the identification of hot/cold gas interfaces as a major impediment to pressure wave suppression. In the acoustic limit, it was possible to separately consider effects of duct geometry, attenuator configuration, and the regions of hot reaction products and cold unreacted gas between these regions. Plotted in Fig. 3 is the magnitude of the acoustic reflection coefficient as a function of the reduced disturbance

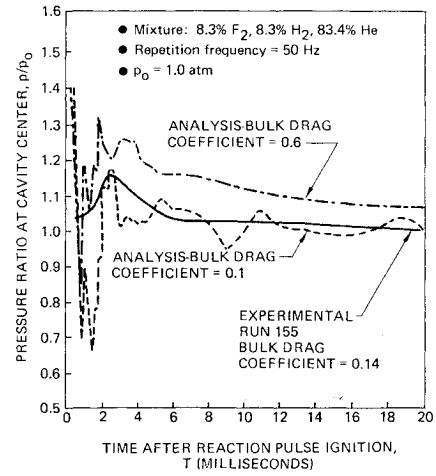

Fig. 4 Comparison of wave suppression analysis and experimental data.

frequency $kh = 2\pi fh/c$, where h is the cavity height, f the disturbance frequency, and c the sonic velocity. Calculated results are shown for various temperature gradients between regions of fixed temperature ratio, $T/T_0 = 1.71$. These results show that decreasing the gradient between hot and cold regions can reduce significantly the reflection coefficient at high frequencies but has little effect on low frequency disturbances. Other calculations showed that reducing the temperature ratio T/T_0 to very low levels was required to reduce the reflection coefficient to 5-10% as required for effective wave clearing. The acoustic transmission calculations showed that cooling of hot reaction products within several cavity lengths downstream of the cavity was required.

The unsteady flow computer program which modeled viscous damping and heat transfer to the attenuator[4] provided the best evaluation of wave suppression techniques of the computational tools available. Heat transfer from gas to damping material is proportional to drag in the model, and internal cooling of the attenuator material is assumed to be adequate to maintain this material at ambient temperature. A number of duct configurations with various damping and heat transfer rates were considered. Results for a configuration that was very similar to the test device, Sec. III, are shown in Fig. 4 (the experimental curve will be discussed in Sec. IV). A 25-cm-long "cavity" located 3 cm downstream of the mixer exit plane and 25 cm downstream of the injector was assumed for these calculations. The modeled area change region was 70 cm long and the total duct length downstream of the cavity was 376 cm, as in the test device. Pressure is shown at the cavity centerline as a function of time after an instantaneous, constant-volume reaction pulse in the cavity that raised the temperature from 292 to 3500 K and the pressure from 1 to 12 atm. Calculated results for two damping rates, $K = 0.1$ and 0.6/cm, are shown in Fig. 4. The pressure uniformity between approximately 6 and 16 ms controls the density uniformity associated with entropy waves. The rms density variation associated with modeled damping rates is considerably greater than 10^{-3}. However, if the linear variation in density is considered to be optically correctable, $\Delta\rho/\rho_{rms}$ for the remaining disturbances when $K = 0.6$/cm is approximately 2×10^{-3} and is near the uniformity requirement. Use of additional damping material is expected to provide a more uniform gas stream exclusive of the linear density variation during cavity filling. The fact that the mean cavity pressure reaches a steady value above ambient conditions for the high damping case is not of particular consequence for device operation. Hence, the unsteady flow calculations show that stationary damping material in an appropriate duct configuration can be expected to provide medium uniformity near $\Delta\rho/\rho_{rms} = 10^{-3}$.

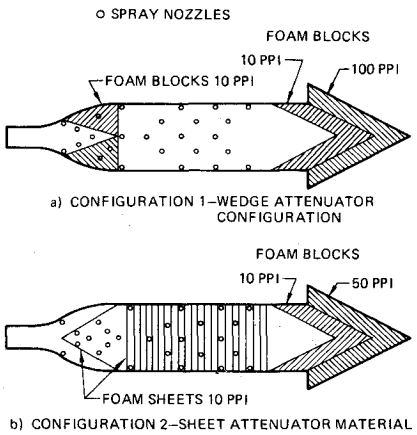

Fig. 5 Schematic of attenuator configuration.

Providing a reliable attenuator with the damping and heat transfer characteristics modeled in the unsteady flow calculations is somewhat of a problem. A large number of relatively small elements must be used to provide the viscous damping required. Cooling and corrosion protection of this attenuator material in the high temperature effluent containing F, F_2, and HF may be feasible but appears to be a very difficult engineering problem.

The attenuation technique developed in this study utilized water sprays of very small droplet diameter to directly suppress the pressure waves and to provide cooling and chemical protection to stationary bulk attenuator material. Analyses of acoustic attenuation in very diffuse water droplet-air systems[5] indicated moderate damping of disturbances with frequencies above 500 Hz in the acoustic range. Published data on droplet drag and breakup in large amplitude unsteady flows[6,7] suggested that momentum, energy, and mass transfer mechanisms would lead to much more effective damping in the large disturbance regime than in the acoustic range. In addition, these data and a simple model showed that much greater number densities of droplets in the 1-10 μm range could be generated and used in unsteady flow situations than in steady flows with acoustic disturbances. Droplet stripping and break-up by the unsteady flow can effectively compete with droplet agglomeration. As will be discussed in Sec. IV, such an attenuator has been developed and pressure wave suppression tests have demonstrated wave attenuation appropriate to $\Delta\rho/\rho_{rms} \leq 10^{-3}$.

III. Test Apparatus and Instrumentation

Tests were conducted in the repetitively pulsed H_2-F_2 flow device shown schematically in Fig. 1. Dimensions of this device along the flow axis were comparable to those of an expected large scale laser device. This insured that the principal pressure disturbances, which occurred along the flow axis, had a frequency content and a wave transmission path which accurately simulated a full scale laser device. Reagents were supplied to the flow channel from blowdown pressure vessels which were sized to have equal 5% supply pressure changes during a test. The H_2 stream was modulated using a 50% on/50% off, rotating ball valve and fast response distribution manifold. As shown in the insert of Fig. 1, H_2 and co-flowing He stream were injected axially into mixing tubes, with F_2-He-O_2 mixture injected transversely to enhance the mixing rate.[8,9] Reactive gas mixture flowed through the central 10×10 cm of a 14×14 cm channel, with a 2 cm thick layer of inert gas separating the H_2-F_2 mixture from the sidewalls. Regions of uniform concentration H_2-F_2 mixture 20-30 cm long were volumetrically initiated by uv radiation from a xenon arc lamp. Tests were performed at pulse repetition frequencies of 50 and 84 Hz, with each run lasting for 15 pulses. F_2/H_2/He mixtures of 4/4/92%, 8.3/8.3/83.4%, and 20/8.3/71.7% with sufficient O_2 to stabilize reaction were used.

An exhaust duct length of 376 cm and area change of 3 was used throughout the reactive flow tests. A smoothly contoured expansion of 140 cm length coupled the 36-cm-long reactor channel to the constant area exhaust duct. Water spray injection rate and nozzle array were not changed during the test program. A caustic water solution containing 5% NaOH by weight was used for all tests to scrub HF and F_2 and to prevent possible violent reactions between the water and fluorine. Stationary attenuator materials (4-40 pores/cm Scott industrial foam) were arranged in two configurations shown schematically in Fig. 5 having a factor of two difference in flow resistance.

The entire exhaust duct-caustic water spray system was a low cost baseline configuration and did not represent an optimized design for either acoustic attenuation, scrubbing, or water mass utilization. The spray nozzles were all aimed downstream parallel to the flow axis and were located near the duct sidewall. Approximately half of the hollow cone spray jet impinged immediately on the adjacent sidewall and was lost. Of the remaining spray which entered the gas stream, droplet trajectory calculations (including viscous drag in the mean reagent stream flow) indicated that most droplets from the small spray nozzles were entrained in the gas flow and provided acoustic damping and cooling. The few large diameter droplets from the small spray nozzles and most droplets from the large nozzles had sufficiently high momentum and low drag to traverse the 14-cm-wide flow channel in 5 ms and were lost on the opposite wall. This portion of the water spray had some cooling and damping benefit while traversing the channel, but would have several times longer residence time and greater effectiveness in the gas stream of a large scale device. Utilization of water spray was very roughly estimated to be 20% for this baseline device. The caustic water mass flow rate was sized to provide adequate water to cool the hot reacted gas stream to 100°C and maintain a small liquid droplet fraction assuming a 20% utilization. Total water mass flow rate was 850 g/s with an effective flow rate of only 170 g/s. More analytical and experimental work needs to be performed to fully characterize and optimize the caustic water spray technique.

Pressure data and interferometric pressure-density calibration experiments provided the basis for the principal conclusions of the experimental program. The experimentally determined dependence of nonisentropic density disturbances (entropy waves) on pressure disturbances discussed in Sec. IV allowed the density nonuniformity at the time of a reaction pulse to be evaluated from pressure data. These data also showed that isentropic (acoustic) density disturbances did not significantly degrade medium optical quality. Great care was taken in instrument selection, mounting design, operation, and recording of data to insure high frequency response, high sensitivity, and high accuracy. All high frequency response pressure measurements were made utilizing Kistler Piezotron transducers Models 201B4, 211B4, 211B5, and 201B5. Frequency response of the B4 and B5 transducers was 100 and 50 KHz, respectively, and maximum resolution was 1.4×10^{-4} and 0.7×10^{-4} atm, respectively. These pressure transducers were mounted in the flow channel wall and were connected to the flow by 1-mm-diameter by 1-mm-long orifices. This recessed mount was necessary to protect the sensing element from radiation and shock heating with minimum degradation of frequency response. The amplifier/cable installation had a frequency response higher than 200 KHz. All pressure data were recorded on magnetic tape using a Sangamo Sabre VI Wideband Group II FM tape recorder having frequency response of 400 KHz. A portion of the pressure data was recorded simultaneously on oscilloscopes. Pressure transducers were located at five positions in the "cavity" and at approximately one meter intervals throughout the attenuator duct. In addition to the piezoelectric transducers, strain gage

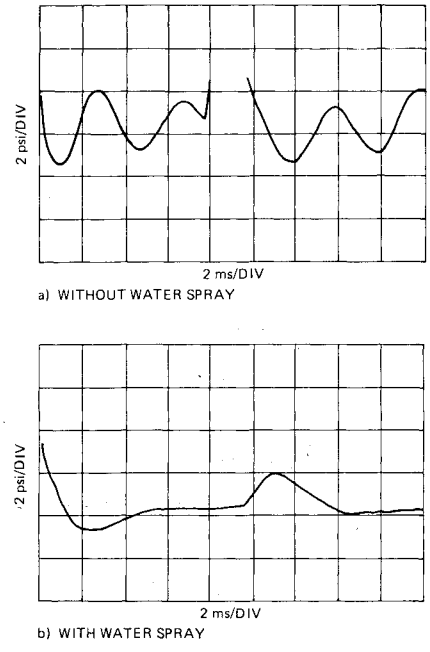

Fig. 6 Pressure histories with and without water spray; bare attenuator channel, and 90% exit blockage.

pressure transducers were used during some tests to monitor long term cavity pressure changes.

IV. Experimental Program Results

Pressure Wave Suppression Using Water Sprays Only

Water sprays provided significant attenuation of higher frequency pressure disturbances and eliminated chemical and thermal problems with the fixed bulk attenuator material. This permitted use of well established pressure wave attenuation materials (e.g., Scott foam) and provided a capability for scrubbing as well. Direct attenuation of pressure disturbances by water spray only is shown in Fig. 6. This figure compares pressure histories between the 12th and 13th reaction pulse of an 8.3% F_2, 8.3% H_2 mixture for the case of a bare channel with (Fig. 6b) and without water spray attenuation (Fig. 6a). A 90% end blockage had been installed at the duct exit during these tests to generate strong waves for interferometric evaluation of entropy wave magnitude. Wave amplitudes both with and without water spray attenuation were quite large for this condition. Peak to peak wave amplitude was damped from 0.51 atm to 0.12 atm. In addition to damping high frequency disturbances associated with the discontinuous pressure rise at ~9 ms in Fig. 6a, attenuation by the water spray almost completely suppressed the large amplitude pressure oscillations of ~4 ms period (~250 Hz) that persisted throughout the pressure trace. Suppression of the lower frequency disturbances by the water spray was due both to acoustic damping and elimination of hot/cold gas interfaces and, consequently, wave reflections from these interfaces. Due to short characteristic times associated with droplet acceleration to the stream velocity, thermal relaxation, and phase change equilibration, water sprays were not particularly effective for damping disturbances of frequencies below 200 Hz. Hence, low frequency disturbances such as that seen in Fig. 6b were expected to persist when water spray alone was used for damping. However, the rapid relaxation rates and high thermal capacity of small water droplets injected throughout the hot gas flow was very effective in cooling the reaction products as indicated by acoustic wave transmit time measurements. In addition to providing useful wave attenuation capability, the water spray eliminated serious materials and cooling constraints that would have otherwise precluded use of bulk attenuators composed of the small diameter materials which are highly effective for acoustic attenuation.

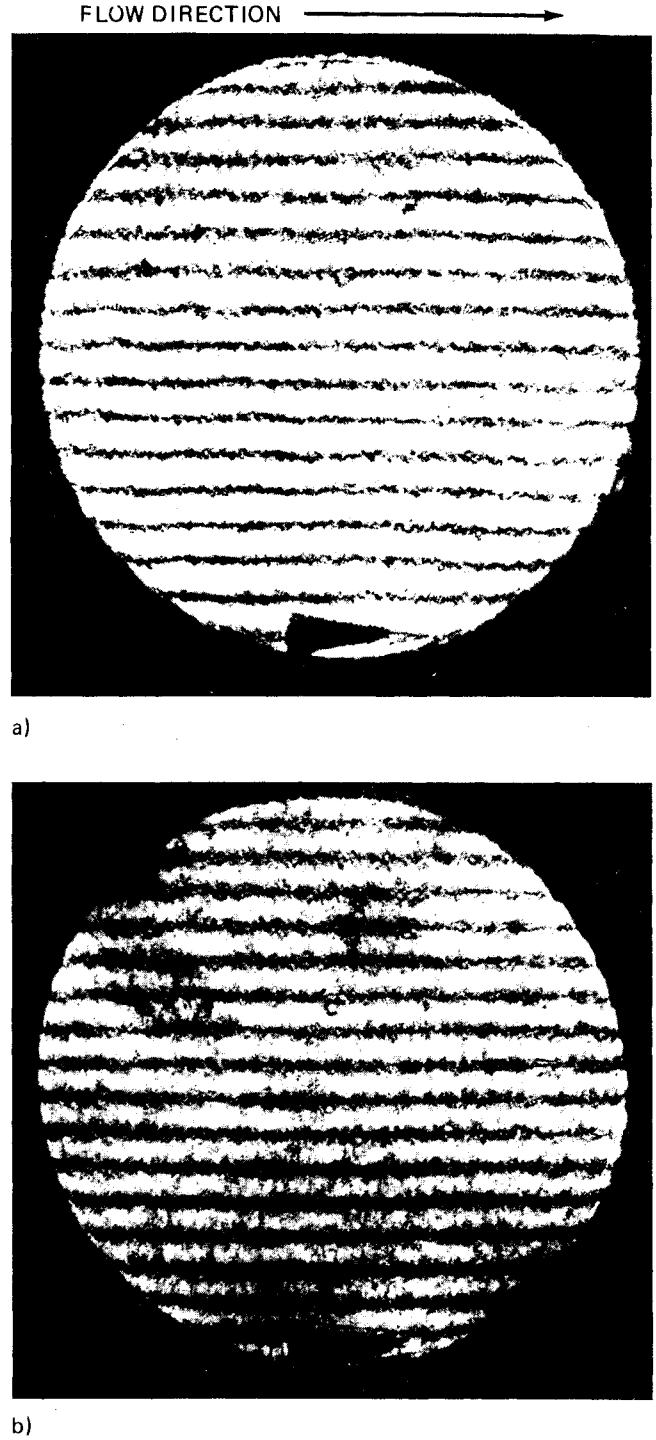

Fig. 7 Interferograms of a) flow at 16 ms after pulse and b) no-flow "reference" conditions. Post-pulse flow was 20% F_2, 8.3% H_2 gas mixture.

Interferometry

A single pass, double pulse, ruby laser holographic interferometer was used to take flow interferograms in a series of tests with a complete pressure wave attenuator (spray and bulk damping material). Windows in the flow channel were 10 cm in diameter and were centered 11.5 cm downstream of the mixer exit plane. The optical path length through the flow channel was 14 cm and the index of refraction of the buffer layers was matched to that of the reagent mixture. Interferograms were taken for 4/4/92, 8.3/8.3/83.4, and

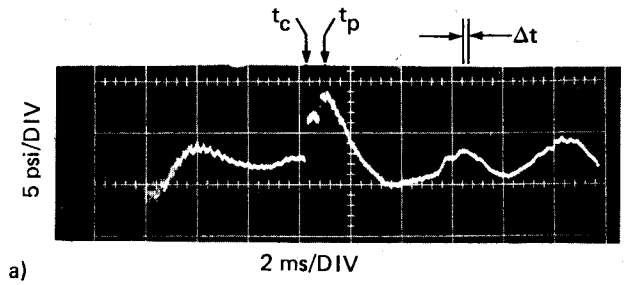

a)

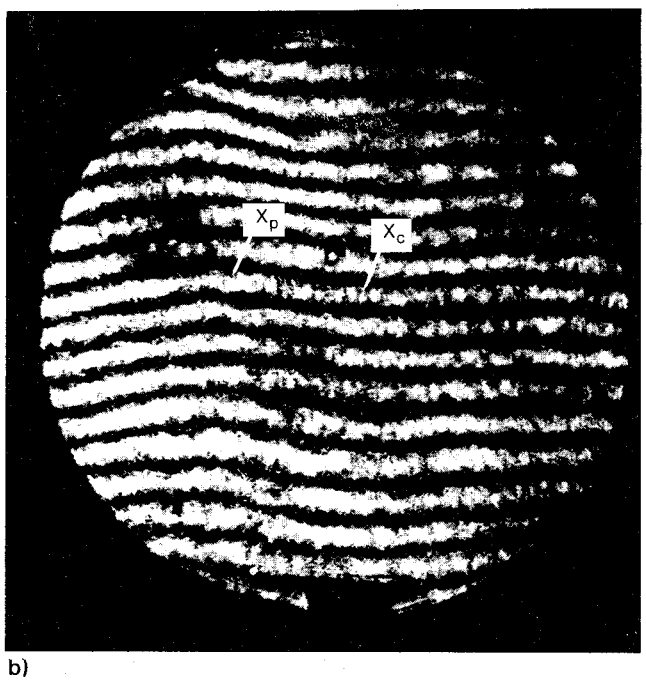

b)

Fig. 8 Interferogram of entropy wave produced by a "probe" pressure wave. a) Pressure transient in cavity. Δt marks pressure distribution in window at time of interferogram. b) Interferogram.

20/8.3/71.7% F_2/H_2/He mixtures after the 12th or 13th pulse. Typical interferograms are shown in Fig. 7 for flow 16 ms after a reaction pulse and for no-flow "reference" conditions. The flow interferogram shown was taken with a 20/8/72% mixture of F_2/H_2/He for maximum sensitivity. It is typical of interferograms taken at various times after pulsed reaction during the period of uniform H_2 cavity fill. Nominally, quiescent air filled the cavity and the remainder of the interferometer path at the reference condition.

Both flow and reference interferograms were of approximately the same quality and showed random nonuniformities on the order of 0.1 fringe or less. None of the interferograms showed flow disturbances that were visible to the eye. To insure that no detectable disturbance was present, both flow and reference interferograms were processed using a high precision microdensitometer readout and computer program that provided a high resolution (0.01 waves) definition of the fringe pattern. In addition, this program evaluated tilt in the flow and vertical directions and subtracted these from the total wavefront nonuniformity to remove distortion introduced by the interferometer wedge used to fix the fringe spacing. The rms wavefront nonuniformity was evaluated for the remaining disturbances. Both flow and no-flow interferograms had rms wavefront nonuniformities of approximately 0.08 wave.

The above results defined the resolution limits of the interferometry as used in this study. Detailed analysis of the no flow interferograms indicated that half the 0.08 wave "noise" was due to window and optical train dust spots, edge diffraction effects, and room vibrations that did not allow complete subtraction of the window distortion effects with the double exposure holographic technique. The other half of the noise level was attributed to random room air currents as they were nonrepeatable in nature. The interferograms with flow showed similar distortions with no entropy wave effects detectable.

These interferometric results can be used to place an upper limit on the minimum detectable density nonuniformity. For an optical path length of 14 cm, and $\beta = 0.8 \times 10^{-4}$ (20% F_2 mix) we have

$$\left(\frac{\Delta\rho}{\rho}\right)_{\text{rms}} < \frac{N\lambda}{\beta L} = \frac{(0.08)(7\times10^{-5})}{(0.8\times10^{-4})(14)} = 5\times10^{-3}$$

Obviously the sensitivity of the interferometry is not sufficient to confirm the achievement of the required flow quality of $\Delta\rho/\rho < 10^{-3}$.

The piezotron pressure transducers used in this experimental study were capable of measuring pressure disturbances over an order of magnitude smaller than the maximum sensitivity of the interferometry. Thus, to confirm that the performance of the pressure wave attenuator was sufficient to support the required $\Delta\rho/\rho < 10^{-3}$, a test was conducted to determine experimentally the relation between the entropy wave density disturbances and the pressure wave disturbances. These data are described in the next section.

Experimental Determination of "Entropy Wave" Amplitude

A series of tests was conducted to determine the dependence of an entropy disturbance on the pressure disturbance which impinged on the injector. Experimental definition of entropy wave amplitude was based on use of interferometry to measure the magnitude of the density disturbance (entropy wave) produced by an induced pressure wave of known amplitude.

An entropy wave of adequate amplitude for good resolution was produced by generating a "probe" pressure wave having desired magnitude and timing relative to other flow events. This pressure disturbance was generated by removing all attenuator material from the exhaust duct, turning off the water spray, and inserting a planar 90% blockage at the duct exit. The associated pressure time history is shown in Fig. 8a. Gas flow through the injector during the time of interaction of this wave with the injector, the convection of the associated entropy wave downstream to the cavity, and deflections of particle paths by pressure disturbances were accounted for in timing the interferogram to coincide with the centering of the entropy disturbance in the window aperture. An interferogram that recorded the entropy disturbance is shown in Fig. 8b. The fringe shift associated with the entropy disturbance was 1.0 wave, which corresponded to a density change of $\Delta\rho_s/\rho \approx 0.09$. Since the amplitude of the pressure variation $\Delta p/p$ producing this entropy wave was 0.41, the functional relationship between the parameters is approximately,

$$\Delta\rho_s/\rho = 0.22(\Delta p/p) \tag{4}$$

Several tests showed repeatability of this constant within $\pm 10\%$.

The difference between the above measured value of K and that derived in Eq. (2) is primarily attributed to the complex geometry of the mixer injector and the inherent unsteady nature of the flowfield. The value $K = 0.38$ was derived on the basis of quasisteady analysis of a single pressure wave interacting with a sonic orifice plate. The Boeing mixer injector consisted of an array of 200 mm long × 4.6 mm i.d. tubes

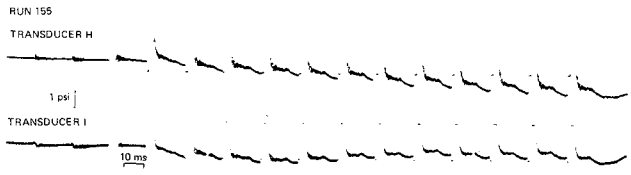

Fig. 9 Multipulse pressure wave suppression with 8.3/8.3/83.4% F_2/H_2/He mixture at 50 Hz using configuration 2 attenuator.

spaced 10 mm apart, providing an area ratio of five between the cavity and mixer flow cross-sectional area. A pressure wave impinging on this area change generates a reflected and transmitted wave as well as a entropy layer. The transmitted wave suffers a small amount of attenuation in the mixing tubes before interacting first with the F_2/diluent orifice located in the tube sidewall (see Fig. 1) and then, 50 mm further upstream, with the H_2-He orifices. Two entropy layers are thus generated. These entropy layers, as well as others generated by other unsteady waves, spread and mix together due to the velocity profile of the turbulent flow in the tubes. (Interface spreading in the mixing tubes was shown to be an important factor in smearing the H_2 on/off interface; see Ref. 1.) Other pressure waves are generated as the wave within the tubes re-emerges and as the entropy layers themselves reach the area change between mixing tubes and cavity. It is apparent that many unsteady flow processes occur and that the simple, quasisteady analysis used to derive Eq. (2) may not be accurate for the flowfield immediately downstream of the mixer-injector face where the laser cavity is located. (For example, Hogge[4] derived a value of $K=0.27$ for our flow conditions based on a unsteady acoustic analysis of a simple orifice plate.) Because of the complicated nature of the unsteady flowfield, the measured value of $K=0.22$ was determined to be more reliable than those derived from linearized and quasisteady analyses and, hence, was used in interpreting the pressure measurements. Furthermore, the measured value for K is specific to the Boeing mixer injector and will be different for other mixer designs.

Pressure Wave Suppression with Full Attenuator

All wave suppression data exhibited characteristics similar to the pressure histories seen in Fig. 9. Of principal interest are data from transducers F, G (not shown), and H, which were located at the cavity center, and transducer I, which was located 15 cm downstream of the cavity centerline. The initial large overpressures of 5-12 atm momentarily saturated the transducer and tape recorder amplifiers during high sensitvity data acquisition. This produced the initially flat negative offset on the H and I pressure traces. Amplifiers returned to normal a few μs after the pressure dropped to a value which did not overload the amplifiers. Pressures returned to nearly uniform conditions in 3-6 ms. The principal disturbance which persisted after 6 ms was a single low frequency pressure wave which entered the cavity between 12 and 15 ms after each pulse, as seen in Fig. 8 and all other 50 Hz test data. This wave was the reflection of the main reaction produced shock wave from the attenuator duct termination. The high-frequency noise was due to transducer pickup of mechanical vibrations of the flow channel structure. The principal structural resonant mode affecting the pressure transducers was channel sidewall bending and had a frequency approximately twice that of the transverse pressure waves, as verified by no-flow structural vibration tests. All piezoelectric pressure transducer data exhibited slow, long term drift during pulsed reaction tests which was due primarily to thermal changes of the transducer sensing element. This condition is evident in the H trace of Fig. 9. Pressure measurements were made concurrently with strain gage transducers to monitor long term cavity pressure changes. Strain gage transducer construction and installation several centimeters from the hot gas stream minimized thermal effects on these transducers. The strain gage pressure data showed that the mean cavity pressure was constant after the first few pulses. The slow, low amplitude drift of the piezoelectric transducers did not measurably affect the rms pressure fluctuation computed in the data reduction, but did introduce a small error, $\pm 3\%$, to the linear component of pressure variation. Data from the first ten pulses of each test were monitored to ensure that a steady operating condition was established and that periodic pressure histories following each pulse had been achieved. However, only data from the 11th to 15th pulse, when periodic operation was always evident, were used for data reduction.

The wavelength of all pressure disturbances remaining after the first 6 ms was several meters or more, i.e., many times larger than the corresponding laser cavity dimensions. Maximum pressure variation during the period between 6 and 20 ms after reaction was on the order of 0.02 atm. Acoustic (isentropic) density disturbances seen in the cavity aperture at the instant of the laser pulse were associated with pressure variations which were small with respect to the maximum variation over the full wave. For conditions achieved during this program, cavity acoustic disturbances were on the order of $\Delta\rho_a/\rho = 10^{-4}$ or less, and were insignificant. However, density disturbances in the form of entropy waves were produced by these low-level pressure waves. A relatively straightforward procedure based on Eq. (4) was followed to evaluate the expected density nonuniformity from the pressure data.

Pressure data from the 10th to 15th pulse were used to evaluate flow uniformity. Data reduction was based on use of a linear regression analysis to determine the linear component of the pressure change between 6 and 20 ms (3.5 and 11.9 ms) after each reaction pulse for 50 Hz (84 Hz) operation. These times correspond to filling of a 30-cm-long cavity volume. An rms pressure variation about this line was determined by integration of the difference between actual pressure history and the linear variation. The linear (tilt) and rms pressure variations for flow test conditions are summarized in Table 1.

Evaluation of several test results between the 10th and 15th pulse demonstrated that the slope of the linear pressure variation was repeatable within $\pm 3\%$. Since the linear component was repeatable and is easily corrected optically, its magnitude is not of significance, but is included in Table 1 for completeness. Increased damping for configuration 2 relative to configuration 1 slowed the overall cavity pressure decrease and consequently increased the tilt component during cavity fill. More importantly, increased damping decreased the

Table 1 Summary of wave suppression data

Configuration	PRF,[a] Hz	F_2/H_2/He, %	$(\Delta p/p)_{\text{tilt}}$	$(\Delta\rho/\rho)_{\text{tilt}}$	$(\Delta p/p)_{\text{rms}}$	$(\Delta\rho/\rho)_{\text{rms}}$
1	50	4/4/92	0.0044	0.0009	0.0048	0.0010
1	50	8.3/8.3/83.4	0.0119	0.0024	0.0071	0.0014
1	50	20/8.3/71.7	0.0227	0.0045	0.0107	0.0021
2	50	8.3/8.3/83.4	0.0253	0.0051	0.0032	0.0006
2	84	4/4/92	0.0210	0.0042	0.0019	0.0004

[a] Pulse repetition frequency.

amplitude of reflected waves and consequently the rms pressure variation. Table 1 also contains the linear and rms components of density variation associated with entropy waves produced by residual pressure disturbances in the full water spray and fixed attenuator system. Density nonuniformity was calculated from the corresponding pressure fluctuations utilizing Eq. (4). The associated density nonuniformities using the configuration I attenuator meet the expected requirements for a pulsed chemical laser medium. Density uniformity was significantly better than required when the attenuator with higher damping, configuration 2, was used.

Comparison of Analysis and Test Results

Results of an unsteady flow analysis have been compared with the pressure history data in Fig. 4. The calculations used in this comparison were made by Poseidon Inc. using the unsteady flow code developed for ARPA.[4] As discussed above, this code includes viscous damping and heat transfer for a cooled, bulk attenuator but does not explicitly model the effect of water sprays. The code calculations model a duct configuration incorporating an internally cooled bulk drag attenuator. The modeled bulk attenuator extended from the horn entrance to the exhaust duct exit. The bulk damping coefficient increased gradually from zero at the horn entrance to a specified value at the horn exit. Damping was constant at the specified value throughout the constant area duct section. The modeled attenuator was very similar to the configuration 2 attenuator which had an average bulk drag coefficient due to stationary material of approximately 0.14/cm.

Calculated and experimental results for a F_2:H_2:He mixture ratio of 8.3:8.3:83.4% are compared in Fig. 4 for 50 Hz operation. Experimental and calculated pressure histories shown are taken at the cavity centerline. Although the calculated and measured pressure histories are in general agreement, experimental pressure histories are much smoother than the calculated histories. These differences are believed to be primarily due to effects of water spray in the experiment which were not modeled. This issue could not be directly resolved experimentally since, as was actually demonstrated in a single run, the fixed attenuator material was quickly destroyed when used without water spray. When used with water spray the attenuator material was not degraded by several thousand reaction pulses. Lack of pressure oscillations about the relatively linear, long term pressure decay observed in experiments is appropriate to much higher damping than the value of 0.14/cm provided by stationary material in this device. This is due in part to direct pressure disturbance damping by the dense water droplet field. However, the large, slow decay of cavity pressure toward ambient conditions and the rise in mean cavity pressure predicted for high damping utilizing only stationary material, shown by the 0.6/cm curve in Fig. 4, was not observed in the experimental data. The lack of significant mean flow resistance due to the water spray does not preclude enhanced pressure disturbance suppression by viscous dissipation.

V. Summary

Techniques for rapidly suppressing pressure disturbances following a pulsed chemical laser reaction pulse have been evaluated analytically and experimentally. An attenuator duct using water sprays and stationary bulk damping material has been developed and tested at repetitively pulsed reaction conditions for a range of reagent mixtures. Attenuation of pressure disturbances from initial overpressures of up to 12 atm to rms pressure fluctuations of $\sim 4 \times 10^{-3}$ atm, exclusive of linear variation, has been demonstrated for a range of reagent mixtures and operating conditions. Elapsed times for disturbance suppression were approximately one fourth of the total pulse period, i.e., ~6 ms at 50 Hz and ~3.6 ms at 84 Hz, as required for 50-60% mass utilization efficiency. Interferometry and pressure measurements were used to experimentally determine the relationship between the residual pressure disturbances and their associated entropy wave density nonuniformities. This relationship was used to verify that the pressure wave attenuation was sufficient to achieve a $(\Delta\rho/\rho)_{rms} < 10^{-3}$. The demonstrated flow system performance opens the way to development of large scale, multipulse, chemical lasers with near diffraction limited optical quality.

Acknowledgments

This work was sponsored in part by the Department of Defense with technical monitoring by S. K. Searles (Naval Research Laboratory), and in part by the Boeing Aerospace Company.

References

[1] Thayer, W. J. III, Buonadonna, V. R., Sherman, W. D., and McClure, J. D., "Pulsed Chemical Laser Flow Technology-Final Technical Report," Boeing Doc. D180-24039-1, Jan. 1978.

[2] Beckmeyer, R. J. and Eversman, W., "Computational Methods for Studying Acoustic Propagation in Nonuniform Wave Guides," *Aeroacoustics: Jet and Combustion Noise; Duct Acoustics*, MIT Press, Cambridge, Mass., 1975, pp. 455-469.

[3] Mays, R. A., "Inlet Dynamics and Compressor Surge," *Journal of Aircraft*, Vol. 8, April 1971, pp. 219-226.

[4] Hogge, H. D. and Crow, S. C., "Gas Dynamics of Pulsed Chemical Lasers," Poseidon Research Rept. No. 8, Sept. 30, 1977.

[5] Marble, F. E. and Chandel, S. M., "Acoustic Attenuation in Fans and Ducts by Vaporization of Liquid Droplets," *AIAA Journal*, Vol. 13, May 1975, pp. 634-639.

[6] Ranger, A. A., "Shock Wave Propagation Through a Two-Phase Medium," *Astronautca Acta*, Vol. 17, 1972, pp. 675-683.

[7] Reineke, W. G. and Waldman, G. D., "Shock Layer Shattering of Cloud Drops in Reentry Flight," AIAA Paper 75-152, Jan. 1975.

[8] Smoot, L. D. and Fort, L. A., "Confined Jet Mixing with Nonparallel Multiple-Port Injection," *AIAA Journal*, Vol. 14, April 1976, pp. 419-420.

[9] Hartung, K. H. and Hibby, J. W., "Beschleunigung Der Turbulenten Mischung in Rohren," *Chemie-Ingenieur-Technik.*, Vol. 44, Jan. 1972, pp. 1051-1056.